# Calculations of fusion capture of breakup fragments of the weakly bound projectile $^{11}$Be with several targets*

A. Gómez Camacho[1†] J. Lubian[2‡]

[1]Departamento de Aceleradores y Estudio de Materiales, Instituto Nacional de Investigaciones Nucleares, Ciudad de México 11801, México

[2]Instituto de Fisica, Universidade Federal Fluminense, Niteroi 24210-340, Brazil

**Abstract:** Calculations of the effect of the breakup reactions of the weakly bound projectile $^{11}$Be on total, complete, and incomplete fusion with targets $^{16}$O, $^{28}$Si, $^{58}$Ni, $^{144}$Sm, and $^{209}$Bi are presented. The calculations primarily focus on the relative effects of projectile neutron and $^{10}$Be fragments on incomplete fusion. In fact, the energy-dependent contributions to the incomplete fusion of the fragments exhibit highly interesting behaviors when targets of different masses and charges are considered. Incomplete fusion for neutron absorption becomes more important than that for $^{10}$Be for all targets at energies around and above the barrier. Indeed, neutron capture becomes increasingly important as the target becomes heavier. In addition, it is found that incomplete fusion becomes larger than complete fusion for energies lower than a certain value that depends on the target. Above this value, complete fusion overcomes incomplete fusion. As a final calculation, an energy-dependent systematic comparison of the total incomplete fusion, incomplete fusion of the neutron, and incomplete fusion of $^{10}$Be for the different targets is presented. The calculations are performed with two complementary theoretical approaches. The continuum discretized coupled channel model is used to determine the relative projectile-target radial wave functions, which are subsequently used in the angular-momentum-dependent model of fusion probabilities to calculate complete, incomplete, and total fusion cross sections.

**Keywords:** weakly bound nuclei, total, complete, and incomplete fusion, CDCC, projected angular fusion distributions

**DOI:** 10.1088/1674-1137/ae71a4 **CSTR:** 32044.14.ChinesePhysicsC.50104102

## I. INTRODUCTION

In recent years, the study of nuclear reactions of weakly bound projectiles with stable targets has been a topic of intense theoretical and experimental research [1−5]. One of the most important aspects of these studies is to comprehend the effects that the breakup channels of the projectile have on other reaction channels such as elastic, transfer, and fusion. Weakly bound projectiles have the characteristic that, when interacting with a target, they break up into several fragments. Basically, this occurs because of the low binding energy of these nuclei. Therefore, new and different fusion processes can be present for such projectiles. Direct Complete Fusion (DCF) is a process that appears when the entire projectile is captured by the target without a previous breakup. There may be cases where the projectile breaks up but, afterward, all fragments are absorbed by the target. This is known as Sequential Complete Fusion (SCF). Thus, the sum of DCF and SCF constitutes Complete Fusion (CF). Experimentally, DCF and SCF are very difficult to distinguish. Another very important fusion mechanism is Incomplete Fusion (ICF). ICF of a given fragment occurs when, following breakup, this fragment is captured by the target while the others fly away to continuum states. Of course, the total ICF corresponds to the sum of all partial ICFs of the fragments. Hence, CF plus ICF determines the Total Fusion (TF) of the weakly bound projectile to the target. Certainly, it is possible that none of the fragments are captured by the target after breakup, which is known as the Non-capture Breakup (NCBU) process. NCBU may take place in several manners. For instance, elastic breakup occurs when the projectile and target remain in their ground states following breakup. In contrast, inelastic breakup occurs when the entire projectile, projectile fragments, and/or target are in excited states be-

Received 26 February 2026; Accepted 19 May 2026; Accepted manuscript online 20 May 2026

* This work has been supported in part by the Brazilian funding agencies CNPq, FAPERJ, and INCT-FNA, Research Project 464898

† E-mail: arturo.gomez@inin.gob.mx

‡ E-mail: jlubian@id.uff.br

fore or after breakup. A full and realistic description of the effects of breakup processes on fusion must consider couplings to all degrees of freedom involved [6]. Furthermore, reactions involving weakly bound nuclei have a higher degree of complexity at sub-barrier energies. This is because, for these projectiles, transfer reactions followed by breakup are essential process that may predominate over direct breakup [7−10]. From a theoretical perspective, studies that consider all of the above breakup excitations become extremely complex. For this reason, and for the sake of reducing the complexity, most theoretical studies consider only the most important reaction channels that could affect fusion, such as elastic, some inelastic, and direct breakup channels. The continuum discretized coupled channel (CDCC) method is possibly the most widely used model for calculating fusion for weakly bound nuclei [11−13]. Using the CDCC model, it is possible to calculate the effects of the continuum breakup states of the projectile on several reaction observables, such as elastic scattering, elastic breakup, and, more recently, fusion. In fact, recent fusion CDCC calculations for weakly bound projectiles with a core-valence structure have been carried out [14−15]. In these calculations, fusion of the core-valence fragments is determined using two short-range absorption potentials, $W_{F_1}$ and $W_{F_2}$, which account for the absorption of the fragments $F_i$, $(i=1,2)$. That is, the $ICF_{F_i}$ of the fragment $i$ corresponds to its capture through the potential $W_{F_i}$. In actual calculations to determine $ICF_{F_i}$, it is supposed that the other fragment is not absorbed, that is, it is transferred to the continuum. In this case, $W_{F_i}\neq 0$ but $W_{F_j}=0$, with $i,j=1,2$, and $i\neq j$. Then, the total ICF of the projectile to the target is $ICF=ICF_{F_1}+ICF_{F_2}$. The CF is determined in a different calculation when the entire projectile is captured without breakup by an absorption potential $W_{PT}$. Although the calculations [16–17] for CF and ICF may be close to experimental data, this approach has a shortcoming, that is, separate calculations are performed for the contributions to the ICF of each fragment and for CF. In this sense, the calculations are not self-consistent. The projected angular-momentum-dependent model of fusion probabilities is a recent model that simultaneously determines the DCF and SCF as well as the ICF of the fragments of valence-core weakly bound projectiles [18−20]. In this model, fusion is not obtained from CDCC calculations, but instead, CDCC is used to obtain the radial projectile-target relative wave functions. These wave functions are, in turn, introduced into the model of fusion probabilities, from which fusion cross sections are calculated. In recent studies, this model was used for calculations of the TF, CF, and ICF of the weakly bound $^{8}$B projectile in reactions with light to heavy mass targets $^{16}$O, $^{27}$Al, $^{28}$Si, $^{58}$Ni, $^{208}$Pb, and $^{209}$Bi [21]. In this study, it was found that ICF is more important than CF for the targets $^{16}$O, $^{27}$Al, $^{28}$Si, $^{40}$Ar, and $^{58}$Ni for incident energies around and below the Coulomb barrier. However, this situation is inverted as the energy increases. That is, at a given energy that depends on the target mass, CF overcomes ICF. For the heavier targets $^{208}$Pb and $^{209}$Bi, CF is the most important component of TF for energies around and above the barrier. In addition, the ICF of the breakup fragments, a proton and $^{7}$Be, of the nucleus $^{8}$B was determined. In fact, a systematic study was performed on the specific contributions to the ICF of the $^{7}$Be and proton fragments for all targets. It was found that the ICF of proton dominates over that of $^{7}$Be for the lighter targets. However, as the mass of the target increases, the contrary occurs. For the heavy targets $^{208}$Pb and $^{209}$Bi, the ICF of $^{7}$Be accounts for most of the ICF for low and high energies. Following similar lines, in this study, a systematic investigation is presented for fusion excitation functions of the neutron-halo weakly bound projectile $^{11}$Be (cluster structure $^{10}\mathrm{Be}+n$, threshold energy $E_{\rm thre}=0.5$ MeV) with targets in a variety of masses. Specifically, CF and ICF cross sections as well as the contributions to ICF from the fragments of $^{11}$Be are determined for reactions with the targets $^{16}$O, $^{28}$Si, $^{58}$Ni, $^{144}$Sm, and $^{209}$Bi. Particular emphasis is placed on determining the relative contributions of CF and ICF to TF as a function of the target mass and incident projectile energy. Similarly, the contributions to ICF from the neutron and $^{10}$Be breakup fragments are investigated as a function of the target mass and incident energy. Experimental data for the ICF of the fragments of $^{11}$Be are scarce, and thus, a comparison of the calculations is not possible. However, from a theoretical perspective, it is interesting to attempt to understand how the neutron and $^{10}$Be fragments may interact with targets of different mass and charge and subsequently be absorbed. The fusion calculations are performed in two steps. (a) The radial wave functions of the relative motion between the incident projectile $^{11}$Be and target are obtained from CDCC calculations. (b) These radial wave functions are, in turn, used in the projected angular-momentum model of fusion probabilities [18−20], from which the cross sections for the different fusion mechanisms are obtained. In Section II, brief descriptions of the CDCC model, which describes breakup states in the continuum of $^{11}$Be, and of the projected angular-momentum model of fusion probabilities are provided. In Section III, details of the construction of the CDCC discrete breakup space of $^{11}$Be are presented. In addition, we present the coupled-channel equations from which the radial wave functions of the projectile-target relative motion are obtained. Finally, the fusion cross sections for the different fusion reaction mechanisms are calculated. Section IV is dedicated to a summary of the results and conclusions.

## II. CDCC AND PROJECTED ANGULAR-MOMENTUM MODEL OF FUSION PROBABILITIES

A complete description of the CDCC model for describing continuum breakup states of the projectile is provided in Refs. [11−13]. This model is applied to quantify the effect of continuum breakup states on several reaction observables. In the present calculations, the CDCC approach is used to determine the radial angular-momentum wave functions of the projectile-target relative motion. These wave functions are, in turn, used in the angular-momentum-dependent model of fusion probabilities. This latter model is described in Refs. [18−21]. A detailed description of the use of the radial wave functions of the projectile-target relative motion obtained by the CDCC model to calculate fusion probabilities is provided in the appendix of Ref. [19].

In the CDCC model, the Hamiltonian of the projectile-target dynamics is expressed as

$$\hat{H}(\boldsymbol{R},\boldsymbol{r}) = \hat{h}(\boldsymbol{r}) + \hat{T} + \hat{U}_1(\boldsymbol{r}_1) + \hat{U}_2(\boldsymbol{r}_2), \tag{1}$$

where $\hat{h}(\boldsymbol{r})$ is the internal Hamiltonian of the projectile, $\hat{T}$ the kinetic-energy operator of the relative motion, and $\hat{U}_1(\boldsymbol{r}_1)$, $\hat{U}_2(\boldsymbol{r}_2)$ are the interaction potentials between the projectile fragments and target. $\boldsymbol{r}_1$ and $\boldsymbol{r}_2$ are the radial distances between the centers of mass of the target and fragment $F_i, i=1,2$, whereas $\boldsymbol{R}$ is the distance from the c.m. of the target to the c.m. of the fragments. Then,

$$\boldsymbol{R} = \boldsymbol{r_2} + \frac{A_1}{A}\boldsymbol{r}, \quad \boldsymbol{r_1} = \boldsymbol{R} + \frac{A_2}{A}\boldsymbol{r}, \quad A = A_1 + A_2, \tag{2}$$

where $A_1, A_2$ are the fragment masses and $A$ is that of the target. The internal Hamiltonian of the projectile is expressed as

$$\hat{h}(\boldsymbol{r}) = \frac{\boldsymbol{p}^2}{2\mu_{\boldsymbol{12}}} + V_{\boldsymbol{12}}(\boldsymbol{r}), \tag{3}$$

where $V_{\boldsymbol{12}}(\boldsymbol{r})$ includes Coulomb and nuclear potentials. The nuclear interaction usually has a volume Woods-Saxon shape. The ground, inelastic, and scattering breakup states of the projectile $\Phi_i$ satisfy

$$\hat{h}(\boldsymbol{r})\Phi_\beta(\boldsymbol{r}) = \epsilon_\beta \Phi_\beta(\boldsymbol{r}), \quad \beta = 0,1,\cdots,N. \tag{4}$$

The interaction potentials $\hat{U}_1(\boldsymbol{r}_1)$ and $\hat{U}_2(\boldsymbol{r}_2)$ in Eq. (1) are expressed as

$$\hat{U}_i(\boldsymbol{r}_i) = \hat{V}_i(\boldsymbol{r}_i) - \mathrm{i}\hat{W}_i(\boldsymbol{r}_i), \; i=1,2, \tag{5}$$

where $\hat{V}_i(\boldsymbol{r}_i)$ are the interactions between the projectile fragments and target, and $\boldsymbol{r}_i$ is the fragment-target distance. $\hat{W}_i(\boldsymbol{r}_i)$ represents the corresponding absorption potential. The total absorption potential is

$$\hat{W}(\boldsymbol{r}_1,\boldsymbol{r}_2) = \hat{W}_1(\boldsymbol{r}_1) + \hat{W}_2(\boldsymbol{r}_2). \tag{6}$$

The total wave function $\Psi^{(+)}$ of the projectile-target nuclear system is obtained by expanding it in terms of the eigenstates of the projectile $\Phi_\beta(\boldsymbol{r})$, $\beta = 0\ldots N$. That is,

$$\Psi^{(+)}(\boldsymbol{R},\boldsymbol{r}) = \sum_{\beta=0}^{N} \psi_\beta(\boldsymbol{R}) \otimes \Phi_\beta(\boldsymbol{r}), \tag{7}$$

where $\psi_\beta(\boldsymbol{R})$ are the radial relative projectile-target wave functions. $\beta=0$ refers to the elastic incident channel, whereas $\beta = 1...N$ denotes the inelastic and excited breakup states. The radial relative wave functions $\psi_\beta(R)$ of Eq. (7) are used to calculate the probabilities of the different fusion mechanisms [18−20]. These wave functions can be determined from CDCC calculations by solving the coupled-channel equations obtained from Eqs. (1) and (7) for a discretized breakup energy space that includes the bound (B) and continuum (C) states of the projectile. These coupled-channel equations are expressed as

$$\begin{aligned}&\left[\hat{T}(R) + U_{\beta\beta}(R) - (E - \varepsilon_\beta - \varepsilon_T)\right]\psi_\beta(R)\\ &= -\sum_{\beta'} U_{\beta\beta'}(R)\psi_{\beta'}(R),\end{aligned} \tag{8}$$

where the coupling matrices are

$$U_{\beta\beta'}(R) = < \phi_\beta \left| \hat{U}_1(\boldsymbol{r}_1) + \hat{U}_2(\boldsymbol{r}_2) \right| \phi_{\beta'} > . \tag{9}$$

Here, $\varepsilon_\beta$ is the excitation energy of the projectile in the $\beta$-state, $\varepsilon_T$ is the ground state energy of the target (assumed to be $\varepsilon_T = 0$), and $U_{\beta\beta}$, $U_{\beta\beta'}$ $(\beta' \neq \beta)$ are the radial dependent diagonal and non-diagonal coupling matrices of the interaction potentials between the ground, inelastic, and continuum breakup states $\beta,\beta' = 0\ldots N$. The CDCC bin states $\phi_\beta(r)$ are defined by square-integrable wave functions as follows:

$$\phi_\beta(r) = \sqrt{\frac{2}{\pi N_\beta}} \int_{k_{i-1}}^{k_i} w_\beta(k) f_\beta(k,r)\mathrm{d}k. \tag{10}$$

This wave packet is generated by superposing radial scattering wave functions $f_\beta(k,r)$, where $f_\beta(k,r)$ is the radial part of $\Phi_\beta(\boldsymbol{r})$ with angular momentum $l$ and parity $\pi = (-1)^l$ in the momentum interval $[k_{i-1},k_i]$, or equivalently, the $[\epsilon_{i-1},\epsilon_i]$ energy interval. $w_\beta$ is a weight function and $N_\beta = \int_{k_{i-1}}^{k_i} w_\beta(k)\mathrm{d}k$ is a normalization constant.

Now, the TF cross-section for a reaction of a weakly bound projectile with a two-particle cluster structure can be written as

$$\sigma_{TF} = \sigma_{DCF} + \sigma_{SCF} + \sigma_{ICF}, \tag{11}$$

where $\sigma_{DCF}$ is the DCF and $\sigma_{SCF}$ is the SCF. Then,

$$\sigma_{CF} = \sigma_{DCF} + \sigma_{SCF} \tag{12}$$

defines the total CF. In turn, the ICF $\sigma_{ICF}$ is expressed as

$$\sigma_{ICF} = \sigma_{ICF_1} + \sigma_{ICF_2}, \tag{13}$$

where $\sigma_{ICF_i}$ $(i = 1,2)$ is the ICF of a given fragment. Note that $\sigma_{DCF}$ is associated with the bound states (B) of the projectile, whereas $\sigma_{SCF}$ and $\sigma_{ICF}$ are associated with the continuum (C) states.

In terms of the bound and continuum states, the total wave function $\Psi^{(+)}$ of Eq. (7) can be split as follows:

$$\Psi^{(+)}(\boldsymbol{R},\boldsymbol{r}) = \Psi^{(B)}(\boldsymbol{R},\boldsymbol{r}) + \Psi^{(C)}(\boldsymbol{R},\boldsymbol{r}), \tag{14}$$

where

$$\Psi^{(B)}(\boldsymbol{R},\boldsymbol{r}) = \sum_B \psi_B(\boldsymbol{R}) \otimes \phi_B(\boldsymbol{r}) \tag{15}$$

and

$$\Psi^{(C)}(\boldsymbol{R},\boldsymbol{r}) = \sum_C \psi_C(\boldsymbol{R}) \otimes \phi_C(\boldsymbol{r}), \tag{16}$$

in which $\psi_B$, $\psi_C$ are the radial projectile-target relative wave functions for the bound and continuum states, and $\phi_B$, $\phi_C$ are the corresponding bound and breakup states of the projectile. In our calculations, it is assumed that the matrix elements of the imaginary potentials connecting the bound and breakup states of the projectile are negligible [14, 22–23]. That is,

$$U_{\beta\beta'}(R) =< \phi_\beta \left| \hat{W}_1(\boldsymbol{r}_1) + \hat{W}_2(\boldsymbol{r}_2) \right| \phi_{\beta'} >= 0, \tag{17}$$

if $\beta$, $\beta' = B, C$, with $\beta \neq \beta'$. Then, the following relations hold:

$$\sigma_{TF} = \sigma^B_{TF} + \sigma^C_{TF}, \tag{18}$$

where

$$\sigma^B_{TF} = \frac{K}{N^2 E} \sum_{\beta\beta' \epsilon B} < \psi_\beta \left| W^{(1)}_{\beta\beta'} + W^{(2)}_{\beta\beta'} \right| \psi_{\beta'} >, \tag{19}$$

and

$$\sigma^C_{TF} = \frac{K}{N^2 E} \sum_{\gamma\gamma' \epsilon C} < \psi_\gamma \left| W^{(1)}_{\gamma\gamma'} + W^{(2)}_{\gamma\gamma'} \right| \psi_{\gamma'} > . \tag{20}$$

Therefore, for the bound states,

$$\sigma^B_{TF} = \sigma^B_{DCF}. \tag{21}$$

This cross-section is constructed by the angular momentum expansion of probabilities to absorb the entire projectile from its bound state, *i.e.*,

$$\sigma^B_{DCF} = \frac{\pi}{K^2} \sum (2J+1)\, \mathcal{P}^{(DCF)}(J), \tag{22}$$

where $K$ is the wave number in the entrance channel and $\mathcal{P}^{(DCF)}(J)$ is provided in terms of the imaginary potential that depends on the projectile-target coordinates, *i.e.*,

$$\mathcal{P}^{(DCF)}(J) = \frac{4K}{E} \int \mathrm{d}r\, W_{PT}(R)\, |\psi_0(R)|^2, \tag{23}$$

where $J$ is the total angular momentum, $\psi_0(R)$ is the radial ground state wave function, and $W_{PT}(R)$ is the projectile-target imaginary potential, without considering the cluster structure of the projectile (the physical reasons for this assumption are discussed in Ref. [20]).

The absorption from continuum states in Eq. (18) is expressed as

$$\sigma^C_{TF} = \sigma_{ICF_1} + \sigma_{ICF_2} + \sigma_{SCF}. \tag{24}$$

In terms of fusion probabilities [20],

$$\sigma_{SCF} = \frac{\pi}{K^2} \sum_J (2J+1)\mathcal{P}^{SCF}(J), \tag{25}$$

$$\sigma_{ICF1} = \frac{\pi}{K^2} \sum_J (2J+1)\mathcal{P}^{ICF1}(J), \tag{26}$$

$$\sigma_{ICF2} = \frac{\pi}{K^2} \sum_J (2J+1)\mathcal{P}^{ICF2}(J), \tag{27}$$

with

$$\mathcal{P}^{SCF}(J) = \mathcal{P}^{(1)}(J) \times \mathcal{P}^{(2)}(J), \tag{28}$$

$$\mathcal{P}^{ICF1}(J) = \mathcal{P}^{(1)}(J)\times\left[1-\mathcal{P}^{(2)}(J)\right], \tag{29}$$

$$\mathcal{P}^{ICF2}(J) = \mathcal{P}^{(2)}(J)\times\left[1-\mathcal{P}^{(1)}(J)\right]. \tag{30}$$

In these equations, $\mathcal{P}^{(i)}(J), i=1,2$ are the probabilities of the fragment $F_i$ being absorbed by the part $\hat{W}_i$ of the imaginary potential (6) independently of what occurs with the other fragment. The expressions of these probabilities are provided in the appendices of Ref. [19].

## III. CALCULATIONS OF CF, ICF, AND TF CROSS SECTIONS

### A. CDCC calculations

In this work, systematic calculations of TF, CF, and ICF of reactions of the weakly bound nucleus $^{11}$Be with targets $^{16}$O, $^{28}$Si, $^{58}$Ni, $^{144}$Sm, and $^{209}$Bi are presented. As a first step, CDCC calculations of the radial projectile-target relative motion wave function $\psi_\beta(R)$, $\beta=0...N$ are performed, which are, in turn, used to determine the fusion probabilities for a given capture process. The FRESCO code [24] is used to solve the coupled-channel equations (8). As is the norm in CDCC calculations, exhaustive convergence tests are performed to solve the coupled-channel equations. Convergence is checked upon changes in the size of the integration step $\Delta r$, matching radius $R_{\max}$, maximum relative angular momentum $l_{\max}$ between the projectile fragments, maximum potential multipole $\lambda$, maximum energy of the bin states $\epsilon_{\max}$, energy width for the construction of the bin states $\Delta\epsilon$, and relative angular momentum of the projectile-target $L_{\max}$. For the calculations of the bound states of $^{11}$Be, the parameters of the nuclear potential $V_{12}(\boldsymbol{r})$ of Eq. (3), which includes a spin-orbit term, are those of Ref. [25]. These parameters yield the correct binding energy of the ground state $1/2^+$, $E_0=0.5$ MeV, first excited state $1/2^-$, $E_x=0.32$ MeV, and resonance $J^\pi=5/2^+$, $E_{\rm res}=1.28$ MeV, with $\Delta E_{\rm res}=100$ keV, for which finer discretization is required. Convergence is achieved with the discretized breakup space described in Ref. [26]: $\Delta r=0.4$ fm, $R_{\max}=40$ fm, bin states constructed up to maximum orbital angular momenta $l_{\max}=4\hbar$, coupling matrix elements up to multipoles $\lambda_{\max}=5$, and maximum energy of bin states up to $\epsilon_{\max}=8$ MeV. It should be noted that some variations in the parameters may be necessary. These variations depend on the incident energy of the projectile and target mass. For instance, the maximum breakup energy $\epsilon_{\max}$ may depend on the incident energy of the projectile. That is, $\epsilon_{\max}$ should be reduced for energies close to or below the Coulomb barrier with respect to energies above the barrier. High excitation states of the projectile can not be reached for low incident energies. However, a parameter that depends on the target is the relative angular momentum of the projectile-target relative motion $L_{\max}$. Fusion for heavier targets may require higher $L_{\max}$ values than that for lighter ones.

### B. Absorption and nuclear potentials

The fusion cross sections (Eqs. (24)−(27)) are calculated using the CF-ICF computer code [27] that determines fusion probabilities in terms of the angular momentum scattering wave functions obtained from the CDCC calculations. The mathematical expressions of the probabilities for the capture of the fragments are provided in the appendix of Ref. [18]. The absorption potentials of the breakup components of the projectile $^{11}\text{Be}\to{}^{10}\text{Be}+n$ (Eq. (6)) are assumed to be Woods-Saxon short-range potentials,

$$W_i(r_i) = \frac{W_0}{1+\exp[(r_i-R_i)/a_0]}, \tag{31}$$

where $i=1,2$, $r_i$ is the distance between the fragment $F_i$ and center of mass of the target (T), and $R_i=r_0(A_i^{1/3}+A_T^{1/3})$, where $A_i$ is the mass of fragment $F_i$. The parameters of the potentials $W_1(r)$ and $W_2(r)$ should be selected such that these potentials are well inside the potential barriers of the fragments and target. For the DCF case, the imaginary potential used in this model is not the sum of the fragment-target potentials, but the projectile-target potential $W_{PT}$. In this case, $A_i$ is replaced with $A=A_1+A_2$. Sequential and incomplete absorption are not zero once either of the fragments, in their trajectories to the target, are inside the absorption potential region. Moreover, the parameters of the fusion absorption potentials $W_{PT}$, $W_1$, and $W_2$ are fixed to the values $W_0=50$ MeV, $r_0=1.0$ fm, and $a_0=0.2$ fm, independently of the target. These potential parameters guarantee that the potentials $W_{PT}(r)$, $W_1(r)$, and $W_2(r)$ are well inside the Coulomb barriers for all targets. For instance, for the heaviest $^{209}$Bi with the projectile $^{11}$Be, the Sao Paulo Potential (SPP) determines a Coulomb barrier positioned at $R_B=11.76$ fm. This value is larger than the absorption potential radius $R=8.157$ fm. This condition is also satisfied for less massive targets. Therefore, the calculations of the fusion cross sections presented later do not depend on the mass of the target. In fact, the independence of fusion cross-sections has been shown in Ref. [28]. The real interactions $\hat{V}_i(\boldsymbol{r}_i)$ of Eq. (5) for the fragments $F_i$, $i=1,2$ with the target include nuclear and Coulomb components. With respect to the nuclear components, we use the SPP [29–30]. Although the code for calculating the SPP also yields the imaginary part, we consider only the real part. The imaginary part is that described above; that is, a short-range absorption potential. In addition, it should be noted that the calculation of the radial SPP allows the option to determine neutron-target potentials.

### C. Fusion cross sections

In this systematic study, our objective is to determine the different fusion processes of $^{11}$Be with targets ranging from light to heavy masses. Of particular interest is the ICF of the neutron and its role in the total ICF cross section as a function of the incident energy of the projectile. Figures 1(a)−(e) show the calculations of CF, ICF, and TF for $^{16}$O, $^{28}$Si, $^{58}$Ni, $^{144}$Sm, and $^{209}$Bi, respectively. As can be observed, from low energies, ICF predominates over CF up to a certain value $E_t$ that depends on the target. In fact, $E_t$ is augmented as the mass and charge of the target increase. For the target $^{16}$O, calculations below the barrier are challenging owing to numerical divergences. However, Fig. 1(a) shows that $E_t$ should be well below that barrier. For the heavier $^{209}$Bi, ICF is larger than CF, so $E_t$ is above the range of energies shown. As the projectile $^{11}$Be approaches the target and enters the region of the attractive nuclear potential on the neutron and the net (Coulomb and nuclear) potential on $^{10}$Be, projectile dissociation can be produced. The attractive nuclear potential on the neutron and net potential on $^{10}$Be become stronger as the mass and charge of the target increase. Consequently, breakup and ICF result in the most important processes for heavier targets. The contrary occurs for light targets. That is, the weaker potentials on the neutron and $^{10}$Be can produce dissociation if the interaction with the target is sufficiently slow, which may occur only for low projectile incident energies. Therefore, as observed, particularly in Figs. 1(a)−(b) for the light targets $^{16}$O and $^{28}$Si, ICF is larger than CF at low energies; however, as the energy increases, CF becomes increasingly important. As shown in Figs.1(c)−(d), as the strengths of the nuclear and Coulomb potentials of the target are augmented, ICF starts to dominate CF for larger energies.

In addition, it is interesting to investigate the individual contributions to ICF from the neutron and $^{10}$Be at low and high energies for the different targets. Figures 2(a)−(e)present the calculations for these contributions to ICF with the targets $^{16}$O, $^{28}$Si, $^{58}$Ni, $^{144}$Sm, and $^{209}$Bi. The calculations show that the ICF of the neutron accounts for most of the total ICF for all targets for energies above the barrier $V_B$. In fact, the neutron ICF contributes more to the total ICF for more massive targets. We can attempt to understand this behavior as follows. Once the projectile breaks up, and for low energies and $L=0$ incident partial waves, the fragment $^{10}$Be must penetrate a barrier during the interaction with the target, whereas the neutron is easily captured (as there is no barrier to penetrate). Therefore, it expected that neutron ICF becomes more appreciable at low and high energies. As the energy increases, $^{10}$Be surpasses the barrier with the target and can be more

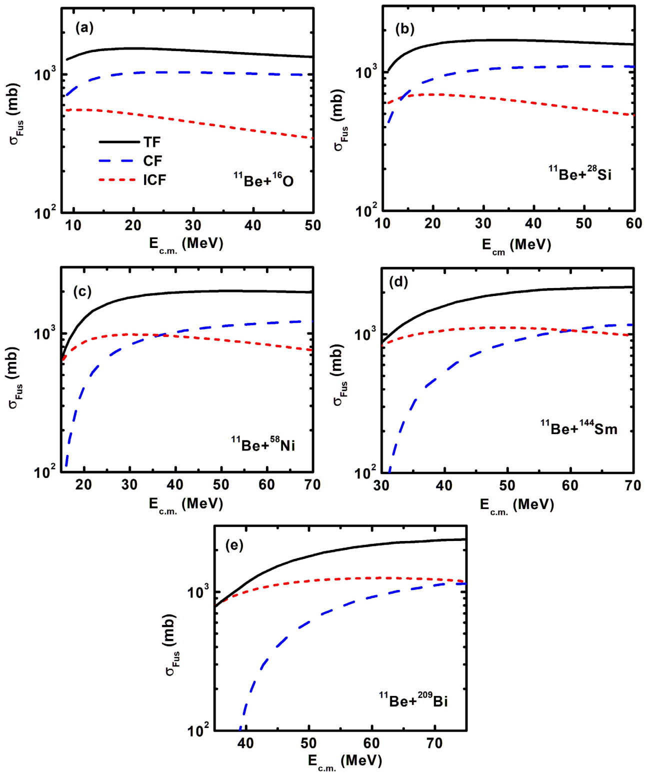


**Fig. 1.** (color online) TF, CF, and ICF cross sections for $^{11}$Be with targets $^{16}$O, $^{28}$Si, $^{58}$Ni, $^{144}$Sm, and $^{209}$Bi.

easily captured. For $L\neq 0$ partial waves, both the neutron and $^{10}$Be must pass through the barrier,

$$V(r) = -V_{\rm nucl}(r) + V_{\rm coul}(r) + \hbar^2 L(L+1)/2\mu r^2, \qquad (32)$$

where, of course, $V_{\rm coul}(r)=0$ for the neutron, $\mu$ is the reduced mass, and $r$ is the fragment-target distance. For low $L$ values, the barrier of $^{10}$Be is higher than that of the neutron. Thus, for energies close to but above the barrier, ICF of the neutron is larger. In fact, as seen in Figs. 2(a)−(e), it is even larger for more massive targets. Now, as $L$ takes bigger values, the pocket barrier for the neutron (formed by the nuclear and centrifugal potentials) vanishes at a certain energy. Then, neutron ICF starts to decrease. However, for $^{10}$Be, the pocket formed by the potentials of Eq. (32) starts to flatten for even larger values of $L$, where fusion is still possible for high energies. This is why, in Figs. 2(a)−(e), fusion of $^{10}$Be increases for higher energies.

In Figs. 3(a)−(d), comparative calculations are shown for the (a) total ICF, (b) neutron ICF, (c) $^{10}$Be ICF at low energies, and (d) $^{10}$Be ICF at energies well above the barrier. The comparison is presented for the different targets as a function of $E_{\rm c.m.}-V_B$, with $V_B$ being the Coulomb barrier of the projectile $^{11}$Be and the target. It can be observed that Figs. 3(a) and 3(b) show similar behavior, i.e., total ICF is basically determined by neutron capture. That is, ICF of the neutron becomes larger for heavier targets.

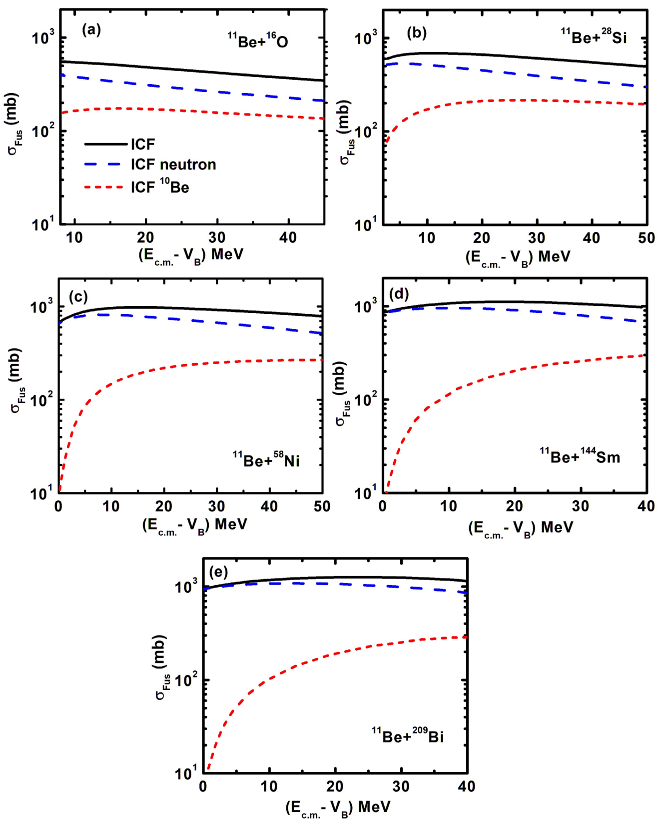


**Fig. 2.** (color online) Neutron, $^{10}$Be, and total ICF cross sections for $^{11}$Be with targets $^{16}$O, $^{28}$Si, $^{58}$Ni, $^{144}$Sm, and $^{209}$Bi. $V_B$ is the barrier energy of the projectile $^{11}$Be and the target.

This is because the attraction on the neutron becomes stronger while repulsion on $^{10}$Be becomes stronger. With respect to the ICF of $^{10}$Be shown in Figs. 3(c)–(d) for low and high energies, this behavior can be understood in the following manner. For low energies and a low incident angular momentum $L$, $^{10}$Be must pass through the barrier of Eq. (32) to fuse with the target. This barrier becomes higher as the target becomes heavier. Table 1 presents the barrier parameters for the various targets as determined by the SPP code [29–30]. Therefore, the ICF of $^{10}$Be for the heavier targets is lower than that for the lighter ones, as observed in Fig. 3(c). For higher energies above the barrier, the deeper nuclear potential $V_{\text{nucl}}$ of massive targets causes the barrier pocket produced by the potentials of Eq. (32) to still be present for a large angular momentum $L$. Therefore, fusion can occur for heavy targets at higher energies. This is not the case for light targets with weaker nuclear potentials, for which the pocket vanishes for lower values of $L$. The results of these calculations are shown in Fig. 3(d). As a final calculation, Figs. 4(a)–(b) show the energy-dependence contributions to the total CF from the direct and sequential components for $^{11}$Be with the light $^{28}$Si and heavy $^{209}$Bi targets. For both targets, the basic component of the CF is DCF. CF predominantly occurs through the ground state of the pro-

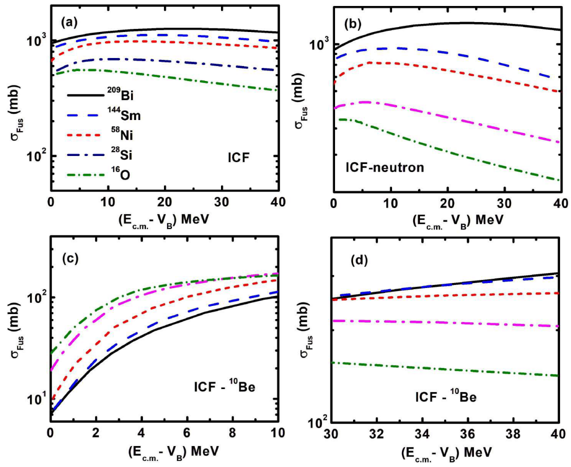


**Fig. 3.** (color online) Comparison of (a) total ICF, (b) neutron ICF, (c) $^{10}$Be ICF for low energies, and (d) $^{10}$Be ICF for energies well above the barrier. $V_B$ is the barrier energy of the projectile $^{11}$Be and the target.

**Table 1.** Coulomb barrier parameters $V_B$, $R_B$, and $\hbar\omega_B$ for $^{10}$Be with targets $^{16}$O, $^{28}$Si, $^{58}$Ni, $^{144}$Sm, and $^{209}$Bi.

| | $V_B$/MeV | $R_B$/fm | $\hbar\omega_B$/MeV |
|---|---|---|---|
| $^{16}$O | 5.11 | 8.28 | 1.50 |
| $^{28}$Si | 8.58 | 8.64 | 1.93 |
| $^{58}$Ni | 15.89 | 9.40 | 2.65 |
| $^{144}$Sm | 30.79 | 10.84 | 3.62 |
| $^{209}$Bi | 38.55 | 11.64 | 4.58 |

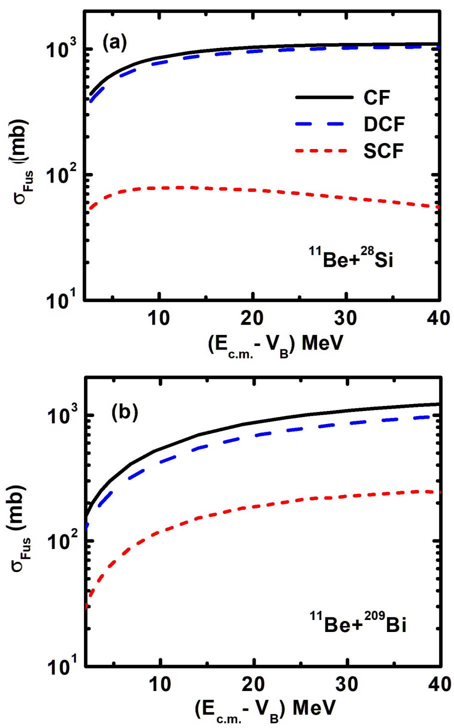


**Fig. 4.** (color online) Total CF, DCF, and SCF for the weakly bound $^{11}$Be with targets (a) $^{28}$Si and (b) $^{209}$Bi.

jectile; that is, direct fusion. It is very interesting to observe that the SCF of $^{209}$Bi becomes increasingly larger than that for $^{28}$Si. This could be related to the stronger potentials that produce breakup of the projectile and then result in capture of the fragments.

## IV. SUMMARY

TF, CF, and ICF cross sections have been systematically studied for the neutron-halo weakly bound projectile $^{11}$Be in reaction with targets $^{16}$O, $^{28}$Si, $^{58}$Ni, $^{144}$Sm, and $^{209}$Bi. The calculations were performed with the CDCC model to determine the radial relative motion wave functions of the projectile-target system. These wave functions were then introduced into the angular momentum-dependent model of fusion probabilities to calculate the excitation functions of the different fusion mechanisms. The results of the calculations led to the following conclusions.

(a) The energy dependence of total ICF becomes increasingly important with respect to CF as the target charge and mass increase.

(b) The contributions to the ICF of the neutron and $^{10}$Be fragments were determined for the different systems. For all targets, the total ICF is mainly due to neutron absorption.

(c) A comparison of the neutron ICF for the different targets showed that, for incident energies above the barrier, the neutron ICF becomes increasingly relevant for more massive targets. In contrast, for the $^{10}$Be fragment, for energies below and around the barrier, fusion becomes smaller for the heavy targets. However, this situation is inverted for high energies, where the ICF of $^{10}$Be increases as the target mass increases.

(d) CF is basically composed of the DCF component at all incident energies. However, for heavier targets, the SCF gradually increases. For light targets, SCF remains very small with respect to DCF.

## References

[1] L. F. Canto, P. R. S. Gomes, R. Donangelo *et al*., Phys. Rep. **424**, 1 (2006)
[2] N. Keeley, R. Raabe, N. Alamanos *et al*., Prog. Part. Nucl. Phys. **59**, 579 (2007)
[3] K. Hagino and N. Takigawa, Prog. Theor. Phys. **128**, 1061 (2012)
[4] B.B. Back, H. Esbensen, C. L. Jiang *et al*., Rev. Mod. Phys. **86**, 317 (2014)
[5] L. F. Canto, P. R. S. Gomes, R. Donangelo *et al*., Phys. Rep. **596**, 1 (2015)
[6] Jin Lei and Antonio M. Moro, Phys. Rev. Lett. **122**, 042503 (2019)
[7] D. H. Luong, *et al*., Phys. Lett. B **695**, 105 (2011)
[8] D. H. Luong, M. Dasgupta, D. J. Hinde, *et al*., Phys. Rev. C **88**, 034609 (2013)
[9] R. Rafiei, R. du Rietz, D. H. Luong *et al*., Phys. Rev. C **81**, 024601 (2010)
[10] A. Shrivastava, *et al*., Phys. Lett. B **633**, 463 (2006)
[11] Y. Sakuragi, M. Yahiro, M. Kamimura, Prog. Theor. Phys. Suppl. **89**, 1 (1986)
[12] Y. Sakuragi, M. Yahiro, M. Kamimura, Prog. Theor. Phys. **70**, 1047 (1983)
[13] N. Austern, Y. Iseri, M. Kamimura, *et al*., Phys. Rep. **154**, 125 (1987)
[14] A. Diaz-Torres, I.J. Thompson, C. Beck, Phys. Rev. C **68**, 044607 (2003)
[15] V. V. Parkar, V. Jha, S. Kailas, Phys. Rev. C **94**, 024609 (2016)
[16] V. V. Parkar, S. K. Pandit, A. Shrivastava *et al*., Phys. Rev. C **98**, 014601 (2018)
[17] H. Kumawat, V. Jha, V. V. Parkar *et al*., Phys. Rev C **86**, 024607 (2012)
[18] J. Rangel, M.R. Cortes, J. Lubian, L.F. Canto, Phys. Lett B **803**, 135337 (2020)
[19] M.R. Cortes, J. Rangel, J.L. Ferreira *et al*., Phys. Rev. C **102**, 064628 (2020)
[20] J. Lubian, J. . Ferreira, J. Rangel *et al*., Phys. Rev. C **105**, 054601 (2022)
[21] A. G. Camacho, J. Rangel, J. Lubian, Phys. Rev. C **111**, 014604 (2025)
[22] G. R. Satchler, M. A. Nagarajan, J. S. Liley *et al*., Ann. Phys. (NY) **178**, 110 (1987)
[23] G. Potel, F. M. Nunes, I. J. Thompson, Phys. Rev. C **92**, 034611 (2015)
[24] I. J. Thompson, Comput. Phys. Rep. **167**, 167 (1988)
[25] P. Capel, G. Goldstein, D. Baye, Phys. Rev. C **70**, 064605 (2004)
[26] J. L. Ferreira, J. Rangel, J. Lubian *et al*., Phys. Rev. C **107**, 034603 (2023)
[27] L.F. Canto, J. Rangel, J. Lubian, CF-ICF computer code (unpublished).
[28] L.F. Canto, R. Donangelo, M. S. H. Hussein *et al*., Phys. Rev. C **98**, 044617 (2018)
[29] L. C. Chamon, D. Pereira, M. S. Hussein *et al*., Phys. Rev. Lett. **79**, 5218 (1997)
[30] L. C. Chamon, B. V. Carlson, L. R. Gasques *et al*., Phys. Rev. C **66**, 014610 (2002)